Size Dependence of Structural Metastability in Semiconductor Nanocrystals

Chia-Chun Chen,* A. B. Herhold, C. S. Johnson,
A. P. Alivisatos,†

The kinetics of a first-order, solid-solid phase transition were investigated in the prototypical nanocrystal system CdSe as a function of crystallite size. In contrast to extended solids, nanocrystals convert from one structure to another by single nucleation events, and the transformations obey simple unimolecular kinetics. Barrier heights were observed to increase with increasing nanocrystal size, although they also depend on the nature of the nanocrystal surface. These results are analogous to magnetic phase transitions in nanocrystals and suggest general rules that may be of use in the discovery of new metastable phases.

In order to expand the range of available solid-state materials, it is important to discover pathways that lead to metastable, high-energy structures. Sometimes, a high-energy form of a solid is observed to persist indefinitely at ambient conditions. For instance, diamond does not revert to graphite under ambient conditions, and high-pressure phases of AlN (*1*) and MgTe (*2*) do not revert to their lower energy phases upon release of pressure. There are many more cases, however, for which dense, high-energy phases of solids, created under conditions of high pressure or temperature, or both, spontaneously transform to a lower energy structure on a rapid time scale. A general understanding of what determines the energetic barriers between crystal structures does not currently exist but is essential for the rational synthesis of new materials. The development of routine syntheses of nanocrystals creates the opportunity to study metastability as a function of a new variable, the size of the crystal (*3*). Such experiments may prove analogous to well-known studies of supercooling in liquid droplets (*4*).

In extended solids, the transformation kinetics and microscopic pathways from one solid structure to another are difficult to determine. First-order, solid-solid phase transitions nucleate at defects, which are present at equilibrium even in the highest quality crystals. As a transformed region of the crystal grows larger, mechanical forces may generate new defects, which in turn act as new nucleation sites. These phase transitions then proceed by complex kinetics involving multiple nucleation and domain fracture (*5, 6*). Thus, it is difficult to compare theoretical calculations of structural stability under pressure to experimental results. For example, theoretical stability calculations of defect- and strain-free bulk Si have shown that it remains metastable in the diamond structure (stable phase under ambient conditions) up to 64 GPa, whereas the thermodynamic transition to the β-tin structure (high-pressure phase) was calculated to be at 8 GPa (*7*). Experimentally, this transformation was observed at 11 GPa (*8*). These discrepancies are the result of differences in barrier heights between simulation and experiment. Thermodynamic calculations do not include a kinetic barrier, and, experimentally, crystalline defects lower the barrier for nucleation.

The kinetics of phase transitions in nanocrystals are simpler than in extended solids because it is possible to make nanocrystals that contain very few defects. In a high-quality sample, each nanocrystal is, on average, a faceted single crystal (*9*). Defects can be annealed out more easily in nanocrystals than in extended solids, because the distance a defect must travel to reach the surface in a nanocrystal is much smaller and the temperature required for annealing is lower (*10*). The effect of any residual defects are restricted to a specific nanocrystal; in contrast, in the extended solid nucleation at defects can propagate the phase transition through a large volume. Furthermore, nanocrystals undergo solid-solid phase transitions by single nucleation events, because the time required for propagation of a phase front across a distance of nanometers is less than the time separation between successive nucleation events in one crystallite (*11–13*).

In this study we investigated the kinetics of the four- to six-coordinate transformation from the wurtzite to rock-salt structure in CdSe and CdS nanocrystals. The transformations were investigated as a function of pressure (0 to 13 GPa) and temperature (300 to 500 K) by x-ray powder diffraction and optical absorption (*14*). We prepared CdSe nanocrystals 23 to 43 Å in diameter, with a narrow size distribution and high crystallinity, according to the methods given in (*15*). The resulting crystallites had wurtzite crystal structure and a faceted, hexagonal shape with an aspect ratio of 1.1:1 (*16*) and were coated with a monolayer of surfactant, tri-*n*-octyl phosphine oxide. The nanocrystals were dissolved in ethylcyclohexane, which was used as the pressure-transmitting medium in a diamond anvil cell (*17*). We also synthesized $Cd_{32}S_{14}(SC_6H_5)_{36} \cdot DMF_4$ (DMF = *N*,*N*-dimethylformamide), which is a monodisperse $Cd_{32}S_{50}$ molecule 15 Å in diameter with zincblende structure, using the methods given in (*18*).

The transformation from wurtzite to rock salt in CdSe nanocrystals is evident in the x-ray powder diffraction patterns (Fig. 1) and occurred at a pressure well above the bulk upstroke transition pressure of 2.8 GPa (*19, 20*). This elevation in transition pressure results from the effects of cluster size on both the kinetic barrier, which scales with the width of the hysteresis of the phase transition, and the thermodynamic transition pressure, which is taken as the center point of the hysteresis loop. Earlier work has demonstrated that the only change in thermodynamic transition point as a function of size arises as a result of differences in the energy at the interface between nanocrystal and pressure medium between the four- and six-coordinate phases (*11*). This causes the entire hysteresis curve to shift to higher pressure in smaller sizes.

To separate kinetic from thermodynamic size effects on the phase transition, we investigated the hysteresis as a function of temperature (Fig. 2). With increasing pressure, the wurtzite unit cell volume decreased smoothly up to a critical pressure, at which point there was an abrupt decrease to the rock-salt unit cell volume as a result of the phase transition. Upon release of pressure, the system recovered to the four-coordinate structure [a mixture of wurtzite and zincblende (*12*)], but at a much lower pressure than the upstroke transformation. The width of the hysteresis is related to the observation time and to the ratio of the barrier height to the thermal energy, k_BT, where k_B is Boltzmann's constant and T is temperature. As the temperature increased from 383 to 433 K, the hysteresis narrowed observably (Fig. 2).

At even higher temperatures the rate of transformation from wurtzite to rock salt became comparable to the observation time, and the kinetics of the structural phase transition were observed directly. In time-dependent measurements (Fig. 3), the

---

Department of Chemistry, University of California, Berkeley, and Materials Sciences Division, Lawrence Berkeley National Laboratory, Berkeley, CA 94720, USA.

*Present address: Department of Chemistry, National Chung-Cheng University, Chia-Yi, Ming-Hsiung 621, Taiwan.

†To whom correspondence should be addressed.

pressure was increased abruptly (within a few seconds), and the phase of the nanocrystals was monitored as a function of time. The transformation was observed to proceed by a single exponential decay, indicating that there is one rate-determining step.

The barrier height at a particular pressure, which can be determined from the temperature dependence of the rate constant by assuming simple Arrhenius kinetics, was found to vary as a function of nanocrystal size, from 0.5 to 2.4 eV per nanocrystal at 4.9 GPa, as the size increased from 23 to 43 Å in diameter (Fig. 4). The barrier at the thermodynamic transition point will be larger than the barrier at 4.9 GPa but should follow the same trend with size (*21*). For small sizes, it appears that the barrier height per CdSe unit is constant, that is, it increases linearly with the number of unit cells. This result is consistent with the expectation that the barrier height is an extensive property of the system and scales with volume (*3*).

The interface between the nanocrystal and the pressure-transmitting medium also influences the barrier height. This contribution is relatively small in the CdSe nanocrystals but dominates in extremely small crystallites. The room-temperature hysteresis of the structural transition in $Cd_{32}S_{50}$ crystallites (Fig. 5) is approximately one-third the width of the hysteresis loop in nanocrystals comprised of 2000 atoms (Fig. 2), consistent with the smaller number of atoms, and thus a small volume contribution to the kinetic barrier. However, changing the composition of the pressure medium substantially alters the width of the $Cd_{32}S_{50}$ hysteresis, demonstrating that the kinetic barrier also depends on the interface. In addition, there is a large shift in the center point of the hysteresis, indicating that the interface energy determines the thermodynamic transition point.

These experiments allow us to understand the size evolution of the kinetic barriers to structural transformations in defect-free solids (Fig. 6). At very small sizes, the barriers are small, as in many molecular isomerizations, and the kinetics are dominated by the interface contribution (*22*). This is clearly the case for the $Cd_{32}S_{50}$ (15 Å in diameter) clusters. As the nanocrystals increase in size, the barriers become substantially larger, and a volume, or interior, contribution dominates. The crossover to interior-dominated kinetics will depend on the chemical composition of the interface but presumably takes place when there is an identifiable core (typically for diameter >20 Å). In this regime, a linear dependence on cluster volume is consistent with models in which a nanocrystal changes phase by coherent deformation of the entire cluster in one step (*3*). A cooperative mechanism of this type also is in accordance with the fact that nanocrystals of 10^2 to 10^3 atoms are smaller than the "critical nuclei" predicted for the bulk solid-solid phase transitions (*6*). At sufficiently large sizes (possibly in the clusters with diameters of 43 Å studied here) the barrier height no longer scales linearly with volume. At these sizes, the kinetics may involve separate nucleation and growth steps,

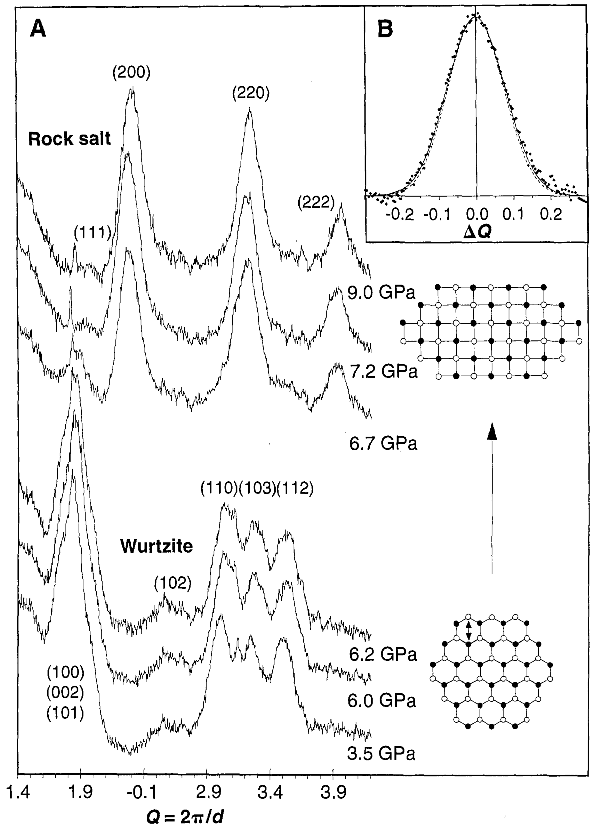

Fig. 1. (**A**) X-ray diffraction patterns with increasing pressure obtained for CdSe nanocrystals 43 Å in diameter at 383 K. $Q = 2\pi/d$, where d is distance in angstroms. The data show an upstroke transformation from wurtzite to rock salt between 6.2 and 6.7 GPa. (**B**) The diffraction linewidths of the nanocrystals, which are inversely proportional to the domain size as a result of Debye-Scherrer broadening, do not change as a result of the phase transition, consistent with single nucleation. The rock-salt diffraction lines at 7.2 GPa (dots) are the same width as the wurtzite lines [solid line, 3.5 GPa, x-ray data; dashed line, atmospheric pressure simulation based on the size determined by transmission electron microscopy (TEM)]. All lines have been shifted to have coincident centers at $\Delta Q = Q - Q_{\text{line center}}$. The proposed transition pathway (*12*) is shown on the right.

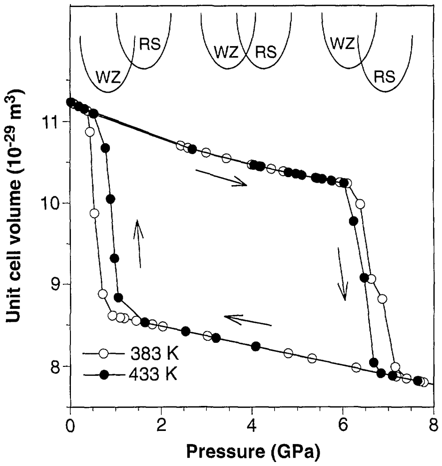

Fig. 2. Hysteresis curves for the four- to six-coordinate transformation in CdSe nanocrystals 43 Å in diameter at 383 K and 433 K. Data were obtained from optical absorption and x-ray diffraction measurements. Arrows indicate directions of increasing and decreasing pressure. We derived the unit cell volumes by integrating the optical absorption features to obtain the fractions of wurtzite (WZ) and rock salt (RS) present and calculating the volume from the data in (*12*). The schematic representation at the top depicts changes in the potential energy curves of the two structures with pressure.

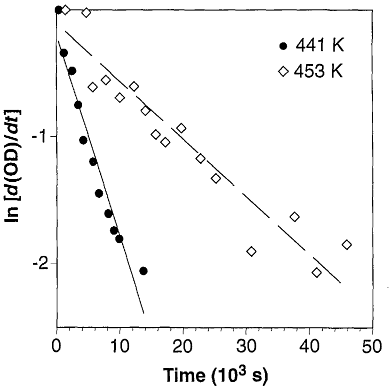

Fig. 3. Transformation from wurtzite to rock salt with time for CdSe nanocrystals 34 Å in diameter at a constant pressure of 4.9 GPa and two temperatures. The differential of optical density (OD) with respect to time (t) was calculated by subtraction of the first absorption feature in the wurtzite phase in two consecutive spectra. The linear fits shown were used to calculate the rate constant at each temperature.

although the barrier height is still large compared to the small cluster limit.

This trend with size does not extrapolate to the bulk solid. Barrier heights in bulk solids are lower than in nanocrystals, mainly because of the influence of defects. For example, the hysteresis width of the transition from wurtzite to rock salt in bulk CdSe is approximately one-third of the width observed in CdSe nanocrystals (*19*, *20*). The size at which more complex bulklike kinetics set in will depend both on the material and on its crystallinity. Highly crystalline Si clusters as large as 500 Å in diameter still demonstrate single nucleation (*13*), and therefore, for the present class of materials, the likely crossover range is 100 to 1000 Å.

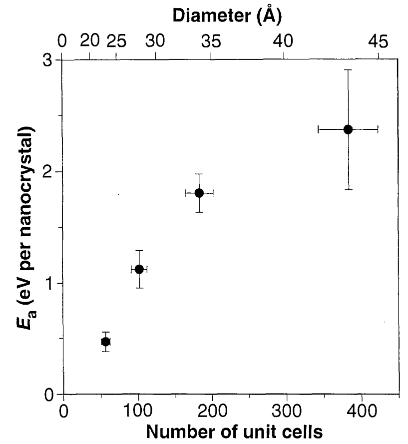

Fig. 4. Changes in activation energy (E_a) versus size (number of unit cells) for CdSe nanocrystals at 4.9 GPa. We calculated the number of unit cells using the sizes obtained from optical absorption measurements and TEM. The volume of a unit cell is 1.124×10^{-28} m^3 obtained from (*12*).

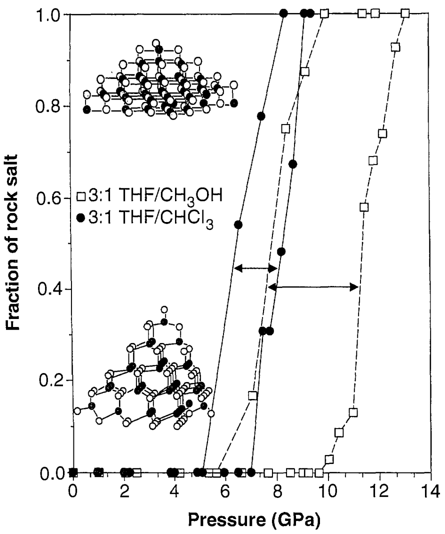

Fig. 5. Hysteresis curves for the four- to six-coordinate transformation in $Cd_{32}S_{50}$ clusters dissolved in two different pressure media. The fraction of rock salt present was determined by integration of optical absorption features. Open squares are for a 3:1 mixture of tetrahydrofuran (THF) and methanol (CH_3OH); filled circles are for a 3:1 mixture of THF and chloroform ($CHCl_3$). Type II diamonds were used to measure absorption spectra down to 250 nm. The model at the bottom represents the structure of a CdS (dark circles are Cd atoms, light circles are S atoms) core cluster (*18*). The model at the top is the predicted rock-salt structure after transformation according to the proposed transition pathway (*12*).

An analogy can be drawn between solid-solid phase transitions in nanocrystals and the well-known magnetic phase transitions in nanocrystals (*23*). Magnetic nanocrystals behave as single domains, which at high temperatures are superparamagnetic and respond to an applied field with no hysteresis. As the system is cooled below the "blocking temperature," the magnetization versus applied field shows hysteresis, including remanence (residual magnetization after the applied field is turned off). The characteristic relaxation time for this hysteresis follows the simple equation

$$\tau_{1/2} \propto \exp\left(\frac{KV}{k_B T}\right) + \text{surface term}$$

where K is the crystalline anisotropy and V is the volume of the crystal (*24*). In crystals above a certain size, multiple magnetic domains are observed, and this equation no longer applies. In solid-solid phase transitions, nanocrystals below a certain size behave as single structural domains, and the kinetic barrier "blocking" the transition can cause the system to be metastable (in analogy to remanence).

We conclude that there is an optimal size to achieve metastability in a solid. This optimal size will depend on the largest size at which single nanocrystals can be prepared defect-free and also on the judicious choice of interface. A much wider range of materials may therefore be metastable in nanocrystals than in extended solids. Examples include high-pressure rock-salt phases stable at ambient conditions in nanocrystalline GaN synthesized under pressure (*25*) and in CdS nanocrystals synthesized in an ionic polymer matrix (*26*). In contrast, high-pressure studies on both bulk GaN (*27*) and CdS (*19*) show that they completely revert from the rock-salt phase to the four-coordinate phase upon release of pressure.

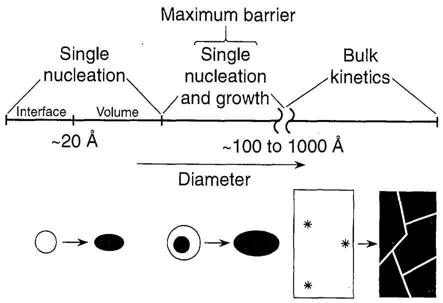

Fig. 6. Illustration of the various size regimes of the kinetics of solid-solid phase transitions. Defects, which act as nucleation sites, are indicated by asterisks in the cartoon of the bulk solid.

Our experiments demonstrate that the kinetics of solid-solid transitions may be understood more clearly in single-domain nanocrystals than in extended crystals. In addition to allowing study of the kinetics, it seems likely that it will be possible to use this technique to investigate additional features of solid-solid phase transitions. For instance, if temperatures sufficiently high compared to the barrier height can be achieved, then the nanocrystals will rapidly fluctuate between the two stable structures on the time scale of the experiments, and the relative populations will be determined by thermodynamics only. It may also be possible to directly determine the detailed dynamics of solid-solid phase transitions in nanocrystals. Indeed, in the limit of finite size, solid-solid phase transitions behave like molecular isomerizations, and a full range of time-resolved techniques may be applied to them.

REFERENCES AND NOTES

1. Q. Xia, H. Xia, A. L. Ruoff, *J. Appl. Phys.* **73**, 8198 (1993).
2. T. Li *et al.*, *Phys. Rev. Lett.* **74**, 5232 (1995).
3. L. E. Brus, J. A. W. Harkless, F. H. Stillinger, *J. Am. Chem. Soc.* **118**, 4834 (1996).
4. D. Turnbull, *J. Chem. Phys.* **20**, 411 (1952); *Solid State Phys.* **3**, 225 (1956).
5. J. M. Besson *et al.*, *Phys. Rev. B* **44**, 4214 (1991).
6. U. D. Venkateswaran, L. J. Cui, B. A. Weinstein, *ibid.* **45**, 9237 (1992).
7. K. Mizushima, S. Yip, E. Kaxiras, *ibid.* **50**, 14952 (1994).
8. J. C. Jamieson, *Science* **139**, 762 (1963); B. A. Weinstein and G. J. Piermarini, *Phys. Rev. B* **12**, 1172 (1975).
9. A well-defined thermodynamic constraint was placed on the system in these studies: An extended crystal may be viewed as having been divided into separate nanometer-size crystals, each of the same size, and with no possibility of atoms migrating between them. Under these conditions, the nanocrystals have a well-defined, size-dependent phase diagram, with an extra term compared to the case for the bulk solid to take account of the surface. This constraint (no communication between crystallites) was carefully observed under all the conditions reported here.
10. A. N. Goldstein, C. M. Echer, A. P. Alivisatos, *Science* **256**, 1425 (1992).
11. S. H. Tolbert and A. P. Alivisatos, *ibid.* **265**, 373 (1994); *Annu. Rev. Phys. Chem.* **46**, 595 (1995).
12. ______, *J. Chem. Phys.* **102**, 4642 (1995).
13. S. H. Tolbert, A. B. Herhold, L. E. Brus, A. P. Alivisatos, *Phys. Rev. Lett.* **76**, 4384 (1996).
14. We achieved high pressures and temperatures using a Merrill-Bassett diamond anvil cell heated in a ceramic oven. The main body of the cell including bolts and screws was made from Inconel 718 to reduce thermal expansion effects, which caused a decrease in pressure of less than 0.5 GPa when experiments were carried out up to 13 GPa and 500 K. We measured pressures using standard ruby fluorescence techniques [J. D. Barnett, S. Block, G. J. Piermarini, *Rev. Sci. Instrum.* **44**, 1 (1973)]. Temperatures were measured with a thermocouple in contact with the steel gasket. High-pressure

and high-temperature x-ray diffraction was performed on wiggler beam line 10-2 at the Stanford Synchrotron Radiation Laboratory with a photon energy of 20 keV. We collected diffraction patterns in the angle-dispersive mode using image plates; these patterns were angle-integrated to obtain the data shown here [J. H. Nguyen and R. Jeanloz, *ibid.* **64**, 3456 (1993)]. In all cases the instrument resolution was far greater than the intrinsic diffraction linewidths because of the small crystallite size. We collected optical absorption spectra using a scanning ultraviolet-visible spectrometer with 2-nm resolution in 6 to 7 min. Optical transitions in wurtzite nanocrystals are electronically allowed, and the absorption consists of a series of discrete features in the visible region. Rock-salt nanocrystals have a band gap in the near-infrared, and the transitions are electronically forbidden but phonon-assisted, as in the bulk material [S. H. Tolbert, A. B. Herhold, C. S. Johnson, A. P. Alivisatos, *Phys. Rev. Lett.* **73**, 3266 (1994)], resulting in a featureless absorption spectrum. We observed an abrupt change in the electronic absorption, a clear signature of the phase transition.

15. C. B. Murray, D. J. Norris, M. G. Bawendi, *J. Am. Chem. Soc.* **115**, 8706 (1993); J. E. B. Katari, V. L. Colvin, A. P. Alivisatos, *J. Phys. Chem.* **98**, 4109 (1994).
16. J. J. Shiang, A. V. Kadavanich, R. K. Grubbs, A. P. Alivisatos, *J. Phys. Chem.* **99**, 17417 (1995).
17. Ethylcyclohexane and the solvent mixtures used for the $Cd_{32}S_{50}$ clusters form glasses between 1 and 2 GPa and behave as hydrostatic pressure media with gradients no greater than 0.5 GPa for the highest pressures obtained in these experiments.
18. N. Herron, J. C. Calabrese, W. E. Farneth, Y. Wang, *Science* **259**, 1426 (1993).
19. A. L. Edwards and H. G. Drickamer, *Phys. Rev.* **122**, 1149 (1961); W. C. Yu and P. J. Gielisse, *Mater. Res. Bull.* **6**, 621 (1971).
20. A. Onodera, *Rev. Phys. Chem. Jpn.* **39**, 65 (1969).
21. In calculating the barrier heights, we assumed that the variations in the thermodynamic transition point with size and temperature were small and could be neglected. The change in the thermodynamic transition point (*12*) is small compared to the full hysteresis width. The pressure dependence of the barrier heights will be discussed elsewhere (C.-C. Chen *et al.*, in preparation).
22. The interface term most likely involves the breaking or rearrangement, or both, of bonds between surface atoms and organic capping ligands and depends on the types of ligands used.
23. E. C. Stoner and E. P. Wohlfarth, *Philos. Trans. R. Soc. London Ser. A* **240**, 599 (1948); L. Néel, *Ann. Geophys.* **5**, 99 (1949); D. D. Awschalom and D. P. DiVincenzo, *Phys. Today* **48**, 43 (1995).
24. F. Bodker, S. Morup, S. Linderoth, *Phys. Rev. Lett.* **72**, 282 (1994); J. P. Chen, C. M. Sorensen, K. J. Klabunde, G. C. Hadjipanayis, *Phys. Rev. B* **51**, 11527 (1995).
25. Y. Xie, Y. T. Qian, W. Z. Wang, S. Zhang, Y. Zhang, *Science* **272**, 1926 (1996).
26. J. Lin, E. Cates, P. A. Bianconi, *J. Am. Chem. Soc.* **116**, 4738 (1994).
27. H. Xia, O. Xia, A. L. Ruoff, *Phys. Rev. B* **47**, 12925 (1993).

28. We thank A. Kadavanich, N. Mizumoto, X. Peng, and M. Schlamp for technical assistance with this project and R. Jeanloz and S. H. Tolbert for helpful discussions. Supported by the Director, Office of Energy Research, Office of Basic Energy Sciences, Material Science Division, of the U.S. Department of Energy (DOE) under contract DE-AC03-76F0098. In these experiments we used the facilities of the University of California–Lawrence Livermore National Laboratory Participating Research Team at the Stanford Synchrotron Radiation Laboratory, which is operated by the DOE, Division of Chemical Sciences.

18 December 1996; accepted 24 February 1997

A Hominoid Genus from the Early Miocene of Uganda

Daniel L. Gebo,* Laura MacLatchy, Robert Kityo, Alan Deino, John Kingston, David Pilbeam

Fossils from a large-bodied hominoid from early Miocene sediments of Uganda, along with material recovered in the 1960s, show features of the shoulder and vertebral column that are significantly similar to those of living apes and humans. The large-bodied hominoid from Uganda dates to at least 20.6 million years ago and thus represents the oldest known hominoid sharing these derived characters with living apes and humans.

Between 1961 and 1965, W. Bishop and colleagues recovered facial, dental, and vertebral remains of a large-bodied hominoid from the Moroto II locality in Uganda (*1*, *2*). Although the dental and facial remains have been interpreted as being primitive [(*1*, *3–7*) but see (*8*, *9*)], the lumbar vertebrae have been considered to be morphologically derived and similar to those of living hominoids, suggesting stiff-backed, orthograde positional behavior like that of living apes and humans (*2*, *10–12*). Thus, the Moroto fossils have remained rather enigmatic, and researchers have been reluctant to associate the primitive teeth and face of the Moroto palate with the derived lumbars, even though all of the elements indicate that the body sizes are similar. In 1994 and 1995, we revisited the East African fossil localities known as Moroto I and II in northeastern Uganda and recovered new hominoid postcranial fossils. These provide additional information about the taxonomy, phylogeny, and functional morphology of the Moroto hominoid.

The fossil-bearing sedimentary rocks at Moroto I and II consist of fluvial and lacustrine sedimentary rocks lying unconformably on Precambrian metamorphic gneisses and capped by a basalt flow. At Moroto II, intercalated coarse- to fine-grained sandstone, conglomerate, siltstone, and mudstone indicate that the depositional environment alternated between fluvial and ponding conditions. Fossils have been found at a number of horizons and are typically associated with medium-grained sandstone and siltstone. Poorly developed paleosols in the sequence suggest that sedimentation was intermittently interrupted. The sequence at Moroto II is up to 38 m thick and is overlain by a fine-grained basalt that presumably flowed down an ancient channel. The sedimentary section at Moroto I is less extensive and consists of a 2.5-m thick section deposited directly on basement and overlain by a basalt. A conglomerate at the base of the exposed section grades up into fine-grained clay, reflecting lacustrine conditions. A paleosol is evident near the top. Fossils are found in both the coarse- and fine-grained deposits.

Assuming that the contact between the basalt and underlying sediments at the two localities defines the same plane, analogous stratigraphic relationships, and similar petrography, it is likely that the basalts represent the same flow. The capping basaltic lavas at Moroto I and II have conventional K/Ar ages of 12.5 ± 0.4 and 14.3 ± 0.3 million years ago (Ma), respectively (*13*). Using faunal correlations, Pickford estimated that the age of Moroto I and II was 14.5 to 16.5 Ma (*14*) and later revised this estimate to older than 17.5 Ma (*15*). To provide firmer dates, we used the ^{40}Ar/^{39}Ar incremental heating technique (*16*). Ages were determined with the use of Fish Canyon Tuff sanidine as the neutron flux monitor (age of 27.84 Ma) (*17*, *18*). The lava from Moroto I gave an internally defined isochron age of 20.61 ± 0.05 Ma (the mean of two experiments). The step-heating spectra for the lava from Moroto II, although demonstrating isotopic disturbance, indicate an emplacement age of more than 20 Ma (Fig. 1).

The fossils from Moroto II [MUZM 80 (MUZM, Makerere University Zoology Museum) (Fig. 2 and Table 1)] consist of several pieces of the right and left femurs of a single large hominoid. We estimate that the length of the femur was 270 mm (*19*, *20*). Several primitive features are present. The

---

D. L. Gebo, Department of Anthropology, Northern Illinois University, DeKalb, IL 60115, USA.
L. MacLatchy, Department of Anatomical Sciences, State University of New York, Stony Brook, NY 11794, USA.
R. Kityo, Department of Zoology, Makerere University, Kampala, Uganda.
A. Deino, Berkeley Geochronology Center, Berkeley, CA 94709, USA.
J. Kingston, Department of Geology and Geophysics, Yale University, New Haven, CT 06520, USA.
D. Pilbeam, Department of Anthropology, Harvard University, Cambridge, MA 02138, USA.

*To whom correspondence should be addressed.